

Kinetic energy and fragment mass distributions for the spontaneous and photon-induced fission of ^{244}Pu

H. Thierens, A. De Clercq, E. Jacobs, M. Piessens, P. D'hondt, and D. De Frenne

Nuclear Physics Laboratory, Proeftuinstraat 42, B-9000 Gent, Belgium

(Received 12 October 1982)

Energy correlation measurements were performed for the spontaneous fission of ^{244}Pu and its photofission with 12-, 15-, 20-, and 30-MeV bremsstrahlung. The photofission cross section for ^{244}Pu was deduced from a measured yield curve up to 30 MeV using the photon difference method. A comparison of the $\langle E_k^* \rangle(m^*)$ behavior for spontaneous and photon induced fission shows that the observed decrease with increasing compound nucleus excitation energy of the average total kinetic energy release is caused predominantly by changes in the total deformation of the fragments for the mass splits with the heavy fragment mass in the vicinity of the closed $N=82$ neutron shell. Comparing the fissioning systems ^{244}Pu and ^{240}Pu , the difference, $\langle E_k^* \rangle_{\text{sf}} - \langle E_k^* \rangle_{\gamma}$, between spontaneous and photon induced fission is 3 MeV larger for the former system. The $\langle E_k^* \rangle(m_H^*)$ curves for ^{240}Pu (sf) and ^{244}Pu (sf) are parallel at a distance of about 3 MeV. The mass distribution for photon induced fission of ^{244}Pu compared to spontaneous fission shows a decreased peak yield, a broadening of the mass distribution peaks, and a shift of the peaks over 3 mass units towards asymmetry. Comparing the fissioning systems ^{240}Pu and ^{244}Pu , the heavy fragment peak remains practically constant in position for both spontaneous and photon induced fission.

| |
|---|
| RADIOACTIVITY, FISSION $^{244}\text{Pu}(\text{sf})$. NUCLEAR REACTIONS, FISSION $^{244}\text{Pu}(\gamma, f)$, $E_{\gamma_{\text{max}}} = 12, 15, 20, 30$ MeV; measured photofission yields, fragment energies E_1, E_2 ; deduced $\sigma(\gamma, f)$, $N(\mu, E_k) / \langle E_{\text{exc}}(E_e) \rangle$. |
|---|

I. INTRODUCTION

It has been shown that shell effects in the nascent fragments play a decisive role in the determination of the fragment mass and kinetic energy distributions.¹ Studies of the excitation energy dependence of these fission characteristics yield information on the rate at which the shell corrections are diminishing and on the coupling of the fission mode to other degrees of freedom. In a previous paper² we reported the results of a comparative study of the spontaneous fission of ^{240}Pu , the thermal neutron induced fission of ^{239}Pu , and the photofission of ^{240}Pu with 12-, 15-, 20-, and 30-MeV bremsstrahlung. Structures in the overall kinetic energy and provisional mass distributions for $^{240}\text{Pu}(\text{sf})$, attributable to the strong influence of the spherical $N=82$ and deformed $N=88$ neutron shells, had already practically disappeared for $^{239}\text{Pu}(n_{\text{th}}, f)$. The excitation energy dependence of the kinematic energy for different mass splits showed that the changes in the total kinetic energy of the fragments in photofission are due to the diminution of shell corrections at

higher excitation energies.

In the present work the kinetic energy and fragment mass distribution for the spontaneous fission and photofission of ^{244}Pu with 12-, 15-, 20-, and 30-MeV bremsstrahlung are compared. For this purpose energy correlation measurements were carried out. Up to now a study of the excitation energy dependence of the mass and kinetic energy distribution for the fissioning system ^{244}Pu was not available. Recently the first results on these characteristics for $^{244}\text{Pu}(\text{sf})$ were reported by Allaert *et al.*³ We measured also the yield curve up to 30 MeV for the photofission of ^{244}Pu and, using the photon difference method described in Ref. 4, we deduced the photofission cross section. This enabled the determination of the average excitation energy of the compound nucleus in the photofission experiments. The changes of the fragment mass and kinetic energy distributions with increasing excitation energy for the systems ^{244}Pu , investigated in these experiments, and ^{240}Pu , studied earlier, are compared. All the results are discussed in the framework of a static scission point model as proposed by Wilkins *et al.*¹

A comparison of the experimentally determined distributions with the results of calculations⁵ following this model is included.

II. EXPERIMENTAL PROCEDURE

For the energy correlation measurements of the spontaneous and photon induced fission of ^{244}Pu a similar experimental setup as described in our paper on the fissioning system ^{240}Pu (Ref. 2) was used. Two Ortec *F* series heavy ion detectors (CF-35-600-60) were mounted symmetrically on both sides of the fission target at an angle of 90° and at a distance of 6 cm to the beam axis. The ^{244}Pu spontaneous fission count rate in this geometry was 90 events per day. The pulse heights of coincident events ($\tau=2$ μs) were recorded in a 4096×4096 channels configuration and stored in blocks of 128 pairs in an INTEL 8085 microprocessor based system, developed in our laboratory. These blocks were transmitted by means of an RS232 line to a VAX 11/780 system. During the photofission runs an on-line correction of the fission fragment pulses for pileup of pulses from scattered γ rays and secondary electrons during the linac pulses (γ flash) was performed as described in a previous paper.⁶ The γ flash was kept below 1% of the pulse heights of the fission fragments by limiting the electron current of the linac. The spontaneous fission measurements were performed during shut-down periods of the linac.

As the spontaneous fission count rate was low and the changes in the kinetic energy of the fragments produced in photofission with bremsstrahlung with different end-point energies are quite small, the stability of the electronics was followed continuously with a precision pulser. In addition, each run at a given bremsstrahlung end-point energy or a spontaneous fission measurement was accompanied by a calibration run with 20-MeV bremsstrahlung. The ^{244}Pu photofission runs with 20-MeV bremsstrahlung were calibrated with $^{241}\text{Pu}(n_{\text{th}},f)$ using the Schmitt *et al.*⁷ calibration procedure and the detector calibration constants of Neiler *et al.*⁸ These calibrations were performed with a well-thermalized and collimated neutron beam of the reactor BR1 of the SCK/CEN, Mol, Belgium, using the same experimental setup as for the ^{244}Pu photofission runs. The stability of the system during these calibration experiments was checked by means of a $^{252}\text{Cf}(sf)$ source and a precision pulser. Based on the $^{241}\text{Pu}(n_{\text{th}},f)$ calibrations and the mass and momentum conservation relations, the data were converted off line in two dimensional provisional mass (μ) and total kinetic energy (E_k) arrays, $N(\mu, E_k)$, of 120×120 channels.

For the determination of the photofission cross

section of ^{244}Pu a yield curve was measured for bremsstrahlung end-point energies between 10 and 32 MeV using the same experimental setup as for the ^{240}Pu yield measurements. No data on the ^{244}Pu photofission cross section below 10 MeV are available in the literature. Based on the similarity of the photofission cross sections between 5.0 and 7.5 MeV for ^{238}Pu , ^{240}Pu , and ^{242}Pu observed by Rabotnov *et al.*,⁹ the behavior of the yield curve for ^{244}Pu from the threshold up to 7.5 MeV was deduced from the ^{242}Pu data of these authors. In the remaining energy region from 8.0 up to 9.5 MeV the yield curve was determined by interpolation between the data of Rabotnov *et al.*⁹ and our data. In the same way as was done for the determination of the ^{240}Pu photofission cross section, the method of Crawford *et al.*⁴ was used for the derivation of the ^{244}Pu cross section, and a normalization using the well known $^{235}\text{U}(\gamma, F)$ cross section¹⁰ was performed.

The ^{244}Pu target consisted of a layer of 29 $\mu\text{g}/\text{cm}^2$ plutonium sandwiched between two 30 $\mu\text{g}/\text{cm}^2$ thick polyimide backings covered with 20 $\mu\text{g}/\text{cm}^2$ gold. The thickness of the plutonium layer of the ^{241}Pu target, used for the calibration, was 40 $\mu\text{g}/\text{cm}^2$. The backing of this target consisted also of a 30 $\mu\text{g}/\text{cm}^2$ thick polyimide foil with 20 $\mu\text{g}/\text{cm}^2$ gold. Both targets were prepared by electro-spraying of plutoniumacetate by the sample preparation group of the Central Bureau for Nuclear Measurements Euratom-Geel (Belgium). The isotopic enrichments of the target materials were 91% for ^{241}Pu and 88% for ^{244}Pu . The contamination of the ^{244}Pu spontaneous fission data with $^{240}\text{Pu}(sf)$ and $^{242}\text{Pu}(sf)$ data was calculated to be 0.5% and 3.4%, respectively.

III. RESULTS AND DISCUSSION

A. Photofission cross section and average excitation energies

The photofission cross section for ^{244}Pu up to 30 MeV obtained from our experiments is plotted in Fig. 1. The error bars on the points indicated in the figure were deduced from the statistical uncertainties on the measured yields. As mentioned in our paper on the photofission of ^{240}Pu (see Ref. 2), a systematic contribution of 10%, mainly due to the uncertainties on the target thicknesses, has to be included to obtain an estimation of the absolute uncertainties on the cross section values.

As generally observed for the actinide nuclei, the giant resonance structure is predominant in the photofission cross section curve shown in Fig. 1. The cross section has a maximum value of 250 mb at 14.0 MeV and a full width at half maximum of 7.1

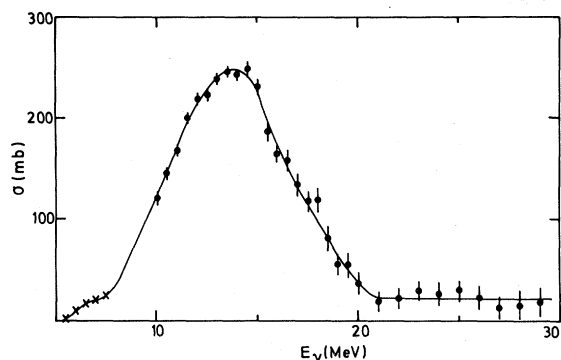


FIG. 1. Photofission cross section of ^{244}Pu , including second and multiple chance fission.

MeV. In the photon energy range above the giant resonance, from 20 to 30 MeV, the cross section is low (20 mb), and constant within the error bars. This behavior was also observed in our study of the photofission cross section of ^{240}Pu . From our experiments we obtained a value of 1.86 ± 0.19 MeV b for the integrated cross section.

The ratio of the fission yields for photofission of ^{235}U and ^{244}Pu with 12-MeV bremsstrahlung, normalized to the same target thickness, was found to be 0.89 ± 0.08 . The study of Caldwell *et al.*¹⁰ of the photonuclear cross section of different actinides in the giant resonance region showed that the total photon absorption cross section is roughly independent of the compound nucleus, and that the ratio of the neutron-emission width to the fission width, Γ_n/Γ_f , is nearly constant above 9 MeV. These conclusions enable us to deduce from the measured ^{235}U to ^{244}Pu photofission yield ratio the value 1.14 ± 0.19

for Γ_n/Γ_f for ^{244}Pu by adopting $\Gamma_n/\Gamma_f = 1.4$ for ^{235}U from Ref. 10. In the work of Caldwell *et al.*¹⁰ the Γ_n/Γ_f values for the different nuclei studied were found to decrease exponentially with the fissibility Z^2/A . Starting from these systematics a value of 0.95 for Γ_n/Γ_f is expected in the case of ^{244}Pu , which is in agreement with the experimentally determined value. The Γ_n/Γ_f ratio deduced from our experiments on ^{240}Pu , 0.63 ± 0.15 , was significantly higher than the expectation value 0.25 following the exponential dependence proposed by Caldwell *et al.*¹⁰ However, for ^{240}Pu this estimation was obtained by an excessive extrapolation of the Z^2/A dependence of Γ_n/Γ_f , deduced from Γ_n/Γ_f values of nuclei with Z^2/A ranging from 34.91 up to 36.17, to a Z^2/A value of 36.82, where for ^{244}Pu the value 36.21 for Z^2/A is very close to the Z^2/A range considered by Caldwell *et al.*¹⁰

Using the Schiff form¹¹ for the bremsstrahlung spectrum and the determined differential photofission cross section, the average excitation energies of the ^{244}Pu compound nucleus, $\langle E_{\text{exc}}(E_e) \rangle$, corresponding to the different end-point energies considered in our experiments, were calculated. The $\langle E_{\text{exc}}(E_e) \rangle$ values for 12-, 15-, 20-, and 30-MeV bremsstrahlung are 9.4, 11.1, 12.5, and 13.2 MeV, respectively. They are nearly the same as those calculated for the photofission of ^{240}Pu .

An estimation of the second chance fission contribution in our ^{244}Pu experiments with 12-, 15-, and 20-MeV bremsstrahlung was calculated from the determined photofission cross section by adopting the ratio of the first-chance photofission cross section to the total photofission cross section for ^{236}U from Caldwell *et al.*¹⁰ We obtained 0%, 8%, and

TABLE I. Parameters of the overall kinetic energy and mass distributions for the spontaneous and photon induced fission of ^{244}Pu .

| | $^{244}\text{Pu}(\text{sf})$ | $^{244}\text{Pu}(\gamma, f)$ | | | |
|--|------------------------------|------------------------------|-------------------|-------------------|-------------------|
| | | $E_e = 12$ MeV | $E_e = 15$ MeV | $E_e = 20$ MeV | $E_e = 30$ MeV |
| Number of fission events | 7990 | 11065 | 24552 | 137842 | 79648 |
| $\langle E_k \rangle$ (MeV) | 180.08 ± 0.30 | 173.58 ± 0.40 | 172.59 ± 0.22 | 171.91 ± 0.20 | 171.63 ± 0.26 |
| $\langle E_k^* \rangle$ (MeV) | 181.79 ± 0.30 | 176.18 ± 0.40 | 175.37 ± 0.22 | 174.83 ± 0.20 | 174.61 ± 0.26 |
| σ_{E_k} (MeV) | 12.62 ± 0.20 | 12.43 ± 0.30 | 12.58 ± 0.34 | 12.68 ± 0.13 | 12.65 ± 0.20 |
| $\langle \mu_L \rangle$ (u) | 106.44 ± 0.19 | 103.83 ± 0.26 | 103.69 ± 0.23 | 103.68 ± 0.16 | 103.91 ± 0.19 |
| $\langle \mu_H \rangle$ (u) | 137.56 ± 0.19 | 140.17 ± 0.26 | 140.31 ± 0.23 | 140.32 ± 0.16 | 140.09 ± 0.19 |
| $\sigma_{\mu_L} = \sigma_{\mu_H}$ (u) | 6.47 ± 0.10 | 7.76 ± 0.11 | 8.01 ± 0.13 | 8.13 ± 0.11 | 8.17 ± 0.17 |
| $\langle m_L^* \rangle$ (u) | 105.96 ± 0.19 | 103.18 ± 0.26 | 103.00 ± 0.23 | 102.92 ± 0.16 | 103.04 ± 0.19 |
| $\langle m_H^* \rangle$ (u) | 138.04 ± 0.19 | 140.82 ± 0.26 | 141.00 ± 0.23 | 141.08 ± 0.16 | 140.96 ± 0.19 |
| P/V | 20 ± 4 | 13.6 ± 2.1 | 12.3 ± 1.3 | 9.1 ± 0.3 | 7.2 ± 0.3 |
| $\langle \nu_T \rangle$ | 2.30 | 3.60 | 3.87 | 4.07 | 4.17 |
| $\langle E_{\text{exc}} \rangle$ (MeV) | 0 | 9.4 | 11.1 | 12.5 | 13.2 |

19%, respectively. As Γ_n/Γ_f is decreasing exponentially with Z^2/A , these estimated values are upper limits for the second chance fission contribution.

B. Kinetic energy

By summing over the total kinetic energy E_k or provisional mass μ , overall provisional mass and total kinetic energy distributions are deduced from the two dimensional $N(\mu, E_k)$ arrays. Some important quantities of the overall kinetic energy and mass distributions are summarized in Table I. The average values of the total postneutron and preneutron kinetic energy and the rms width of the kinetic energy distributions are denoted by $\langle E_k \rangle$, $\langle E_k^* \rangle$, and σ_{E_k} , respectively. The uncertainties on all the values given in Table I are the root-mean-square deviations for at least five experimental runs. For the calculation of the average total preneutron kinetic energy $\langle E_k^* \rangle$ from the measured $\langle E_k \rangle$ value in the case of $^{244}\text{Pu}(\text{sf})$, the measured value 2.30 ± 0.19 of Ref. 12 for the average number of emitted neutrons $\langle \nu_T \rangle$ was used. As for the fissioning system ^{244}Pu , no information on the compound nucleus excitation energy dependence of $\langle \nu_T \rangle$ is available, the $\langle \nu_T \rangle$ values for the photofission of ^{244}Pu were deduced from energy balance considerations using the calculated values of the average excitation energy of the compound nucleus and the $\langle E_k \rangle$ behavior observed in this work. Based on the review paper of Nifenecker *et al.*,¹³ a linear relation between the total γ energy released per fission event and the average number of emitted neutrons $\langle \nu_T \rangle$ was assumed. For the slope of this linear variation, the average value of this parameter for the fissioning systems $^{235}\text{U}(n_{\text{th}}, f)$ and $^{252}\text{Cf}(\text{sf})$, 0.9 MeV/neutron, was adopted. From the same paper we adopted 8.6 MeV for the average energy necessary to emit one additional neutron. The difference in $\langle Q \rangle$ value between the spontaneous fission and photon induced fission case, due to differences in the mass distribution, was also taken into account. For this calculation the charge distribution was assumed to be a Gaussian with a constant value, 0.35, independent of the fragment mass for the variance σ_Z^2 . This assumption was based on the $^{235}\text{U}(n_{\text{th}}, f)$ data of Ref. 14. The maximum of the charge distribution was fixed by the assumption, deduced from the $^{235}\text{U}(n_{\text{th}}, f)$ data of Ref. 15, that the heavy fragment charge is 0.5 charge units higher than the charge following the hypothesis of unchanged charge density of compound nucleus and fragments. The fragment masses were adopted from the tables of Möller and Nix.¹⁶ The values for $\langle \nu_T \rangle$, obtained in this way for photofission, are also given in Table I.

For the comparison of the $\langle E_k^* \rangle$ values obtained in this work for the fissioning system ^{244}Pu with our previously published data on ^{240}Pu (Ref. 2), and with the results of other authors,³ an additional systematic contribution of 1 MeV has to be added to the uncertainties given in Table I due to uncertainties on the thickness of the targets and the calibration procedure. Taking into account this systematic error, our $\langle E_k^* \rangle$ value for the spontaneous fission of ^{244}Pu is in agreement with the value of Allaert *et al.*,³ 184 ± 1 MeV, and is significantly higher than the $\langle E_k^* \rangle$ value for the spontaneous fission of ^{240}Pu , 178.85 ± 0.50 MeV, obtained in our previous work. However, the $\langle E_k^* \rangle$ values for the photofission of ^{244}Pu are the same within the error bars as those for the photofission of ^{240}Pu at the corresponding bremsstrahlung end-point energies. Also the value -0.40 ± 0.10 for the slope

$$d\langle E_k^* \rangle / d\langle E_{\text{exc}}(E_e) \rangle,$$

obtained by a linear fit to the ^{244}Pu photofission data using a weighted least squares procedure, is very close to the value -0.37 ± 0.08 obtained for the photofission of ^{240}Pu . The same behavior of $\langle E_k^* \rangle$ with the compound nucleus excitation energy for the photofission of ^{240}Pu and ^{244}Pu , and the observed difference in $\langle E_k^* \rangle$ for the spontaneous fission of these nuclei, indicate that the difference between the spontaneous and photon induced fission of ^{244}Pu is 3 MeV higher than for the fissioning system ^{240}Pu .

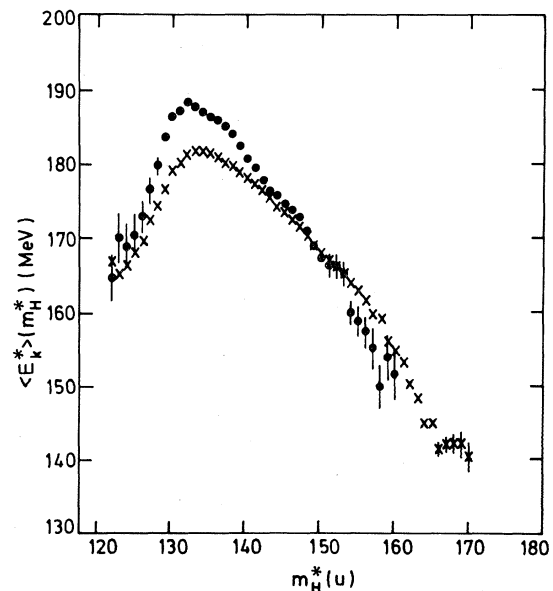


FIG. 2. Average preneutron kinetic energy $\langle E_k^* \rangle(m^*)$ as a function of the heavy fragment mass for $^{244}\text{Pu}(\text{sf})$ (dots) and ^{244}Pu photofission with 20-MeV bremsstrahlung (crosses).

To interpret the observed changes in the average total kinetic energy, the dependence of the total kinetic energy on the fragment mass for the spontaneous and photon induced fission was studied. In Fig. 2 the variation of the average total preneutron kinetic energy with the heavy fragment mass $\langle E_k^* \rangle(m_H^*)$ for the spontaneous fission and 20-MeV bremsstrahlung induced fission of ^{244}Pu is compared. For the derivation of $\langle E_k^* \rangle(m_H^*)$ from the two-dimensional $N(\mu, E_k)$ arrays, the neutron emission curve $\langle \nu \rangle(m^*)$ for $^{241}\text{Pu}(n_{\text{th}}, f)$, deduced by Caïtucoli *et al.*¹⁷ from the provisional and postneutron mass distribution, was adopted as no information on the behavior of $\langle \nu \rangle(m^*)$ for the fissioning system ^{244}Pu is available. In the symmetric fission region, where the neutron yields cannot be determined with the method used in Ref. 17, $\langle \nu \rangle(m^*)$ was determined by linear interpolation between the extreme points around mass 110 and 130 given by Caïtucoli *et al.*¹⁷ This procedure was based on the sawtooth shape of $\langle \nu \rangle(m^*)$ generally observed in low energy fission. The adopted $\langle \nu \rangle(m^*)$ values for $^{241}\text{Pu}(n_{\text{th}}, f)$ were multiplied with an appropriate factor to obtain the correct number of emitted neutrons, $\langle \nu_T \rangle$. For the masses where the error bars are not given in the figure, the uncertainties have the sizes of the points.

Both curves show the typical behavior, with a

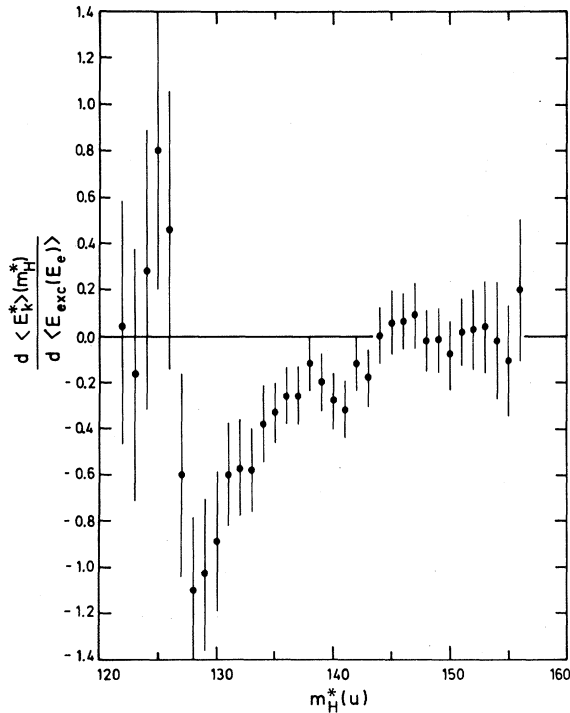


FIG. 3. Variation of $\langle E_k^* \rangle(m_H^*)$ with $\langle E_{\text{exc}}(E_e) \rangle$ for the photofission of ^{244}Pu .

maximum in the mass region of the closed $N=82$ neutron shell, generally observed in low energy fission. In the framework of a static scission point model, as proposed by Wilkins *et al.*,¹ this maximum can be attributed to the low total deformation ($\beta_1 + \beta_2 \simeq 0.95$) of the scission configuration with the heavy fragment at the spherical $N=82$ neutron shell. Comparing the $\langle E_k^* \rangle(m_H^*)$ behavior for the spontaneous fission and 20-MeV bremsstrahlung induced fission of ^{244}Pu , a strong decrease in this $N=82$ neutron shell mass region is present. This decrease can be understood by the enhanced importance, at higher intrinsic temperatures, of a secondary scission configuration with total deformation ($\beta_1 + \beta_2 \simeq 1.4$) close to the one expected from the liquid drop model. In the region around mass 145 the kinetic energy remains practically constant, while for strongly asymmetric mass splits with $m_H > 150$ the kinetic energy is higher in the photon induced fission case. A similar behavior was also observed for the fissioning system ^{240}Pu (Ref. 2). As already mentioned in our previous work,² in the comparative study of Unik *et al.*¹⁸ of the fissioning systems $^{246}\text{Cm}(sf)$, $^{245}\text{Cm}(n_{\text{th}}, f)$, $^{250}\text{Cf}(sf)$, and $^{249}\text{Cf}(n_{\text{th}}, f)$, the kinetic energy was also found to be constant for the mass splits with the heavy fragment mass around 145 and lower for more asymmetric mass splits in the spontaneous fission case. The higher kinetic energy generally observed in this mass region for induced fission compared to spontaneous fission is difficult to explain by changes of the shell corrections at higher intrinsic temperatures.

The variation

$$d\langle E_k^* \rangle(m_H^*)/d\langle E_{\text{exc}}(E_e) \rangle$$

of the total preneutron kinetic energy with the average excitation energy of the compound nucleus as a function of the heavy fragment mass for the photofission of ^{244}Pu is presented in Fig. 3. Also, here a similar behavior as for ^{240}Pu (Ref. 2) is observed, showing that the changes of $\langle E_k^* \rangle$ with the bremsstrahlung end-point energy in photofission can be attributed to the decrease of shell corrections at higher intrinsic temperatures in the mass region around mass 130, resulting in an increasing importance of the liquid-drop favored configuration with larger total deformation. The independence of the kinetic energy on the excitation energy of the fissioning nucleus for the mass splits in regions where shell effects are of minor importance indicates that the fission mode is weakly coupled to quasiparticle excitations and strongly damped, as was pointed out by Nifenecker *et al.*¹⁹

A comparison of the $\langle E_k^* \rangle(m_H^*)$ curves for the spontaneous fission of ^{240}Pu and ^{244}Pu is presented in Fig. 4. Except in the symmetric fission region,

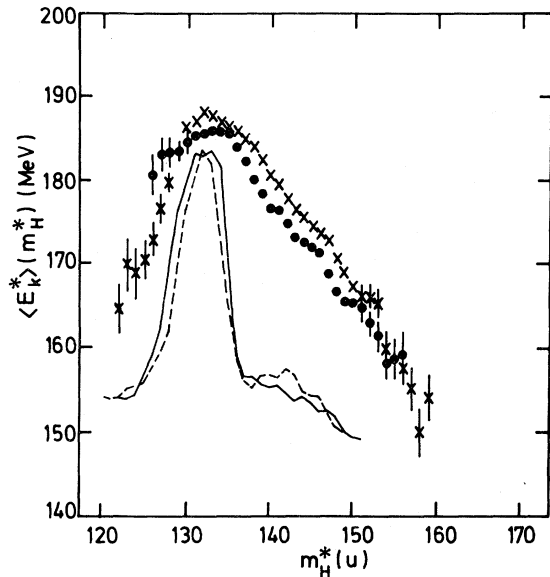


FIG. 4. Comparison of the $\langle E_k^* \rangle(m_H^*)$ curves for the spontaneous fission of ^{240}Pu and ^{244}Pu . The experimental data, obtained in this work for $^{244}\text{Pu}(\text{sf})$, are indicated by crosses. The data for $^{240}\text{Pu}(\text{sf})$, obtained in a previous study (Ref. 2), are represented by dots. The dashed and the solid lines are the results of the scission point model calculations (Ref. 5) for the fissioning systems ^{240}Pu and ^{244}Pu , respectively.

where the comparison is unreliable owing to the poor statistics and the large number of scattered events in the case of $^{244}\text{Pu}(\text{sf})$, the $\langle E_k^* \rangle(m_H^*)$ values for $^{244}\text{Pu}(\text{sf})$ lie systematically above the curve for $^{240}\text{Pu}(\text{sf})$ at an average distance of 2.7 MeV. To investigate whether this difference can be attributed to shell effects in the fragments, the results of scission point model calculations, as proposed by Wilkins *et al.*,¹ are also shown in Fig. 4. For the intrinsic temperature, τ_{int} , the collective temperature, T_{coll} , and the distance d between the coaxial spheroids, the values $\tau_{\text{int}}=0.75$ MeV, $T_{\text{coll}}=1$ MeV, and $d=1.4$ fm proposed by Wilkins *et al.*¹ were adopted. These calculations were performed by Moreau and Heyde.⁵ The comparison of the experimentally determined $\langle E_k^* \rangle(m_H^*)$ behavior with the calculated curves shows that the systematic difference in $\langle E_k^* \rangle$ between the spontaneous fission of ^{240}Pu and ^{244}Pu cannot be attributed to fragment shell effects and is difficult to explain in the framework of a scission point model with a single choice of values for τ_{int} , T_{coll} , and d . More compact scission shapes or/ and a slightly higher pre-scission kinetic energy in the case of $^{244}\text{Pu}(\text{sf})$ are possible explanations for the observed difference. Experimental evidence that the systematic difference between $^{240}\text{Pu}(\text{sf})$ and $^{244}\text{Pu}(\text{sf})$ is not due to localized shell effects can also be found

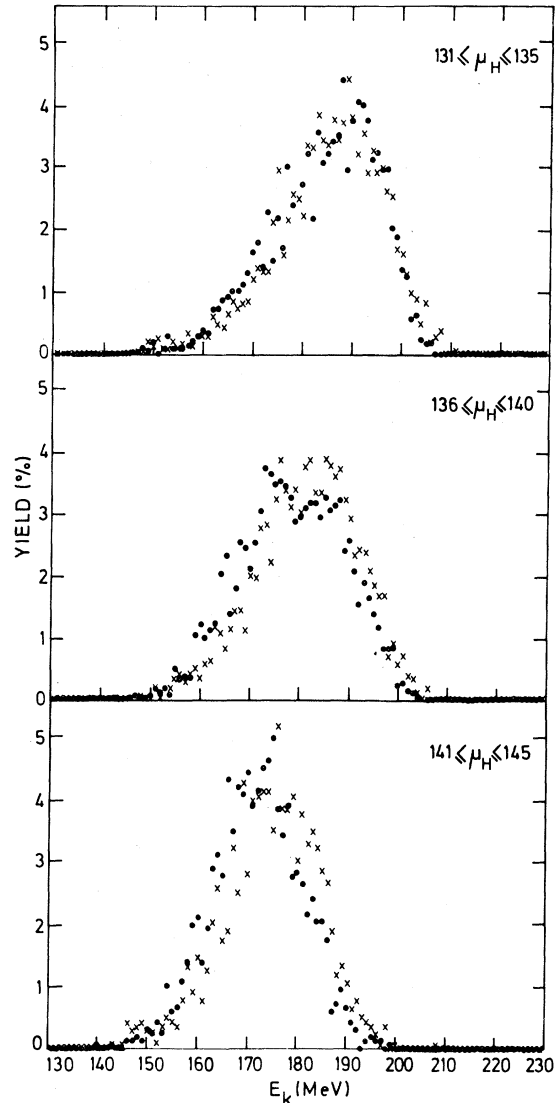


FIG. 5. Comparison of the total kinetic energy distributions for the spontaneous fission of ^{240}Pu and ^{244}Pu for different mass splits, grouped over 5 mass units. The crosses represent the ^{244}Pu data, the dots the ^{240}Pu data. The yields indicated in the figure are obtained by normalization of the total kinetic energy distribution for the considered mass range to 100%.

in Fig. 5, where the total kinetic energy distributions of the fragments with masses in the intervals 131–135, 136–140, and 141–145 are compared. These distributions were normalized to the same total yield. It is apparent from this figure that in the mass ranges 136–140 and 141–145 an overall shift of the whole kinetic energy distribution is present. For the fragments with masses in the range 131–135, the region of the $N=82$ closed neutron shell, this behavior is not observed, which could be

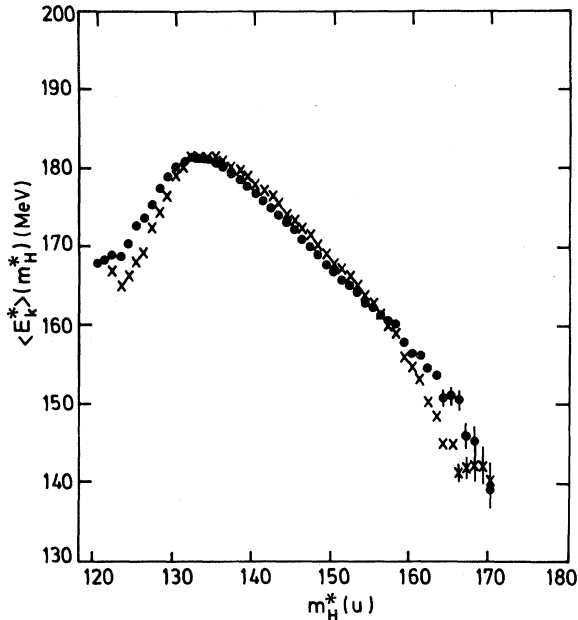


FIG. 6. Comparison of the $\langle E_k^* \rangle(m_H^*)$ curves for the photofission of ^{240}Pu (Ref. 2) and ^{244}Pu with 20-MeV bremsstrahlung. The ^{240}Pu and ^{244}Pu data are represented by dots and crosses, respectively.

owing to changes in the relative contributions of the shell-stabilized configuration with small total deformation and the secondary configuration with higher total deformation close to the liquid drop value.

The comparison of the $\langle E_k^* \rangle(m_H^*)$ curves for the photofission of ^{240}Pu and ^{244}Pu with 20-MeV bremsstrahlung, given in Fig. 6, shows that for asymmetric mass splits the differences between the fissioning systems ^{240}Pu and ^{244}Pu are reduced significantly compared to spontaneous fission. The average value for this difference in the heavy mass range 130–150 is 0.93 MeV. Taking into account the systematic uncertainty of 1 MeV on the kinetic energy in comparing the ^{240}Pu and ^{244}Pu results (owing to the uncertainties on the thickness of the used targets), the difference is negligible. According to our measurements the kinetic energy release in the symmetric fission region is lower for the photofission of ^{244}Pu compared to ^{240}Pu . However, as the contamination of the data by scattered events, caused by the use of an electro-sprayed ^{244}Pu target, is relatively largest in regions with low counting rate, it is not clear that the observed difference for symmetric fission really has a physical meaning.

C. Mass distributions

The important parameters of the mass distributions for the spontaneous and photon induced fission of ^{244}Pu are also given in Table I. The average

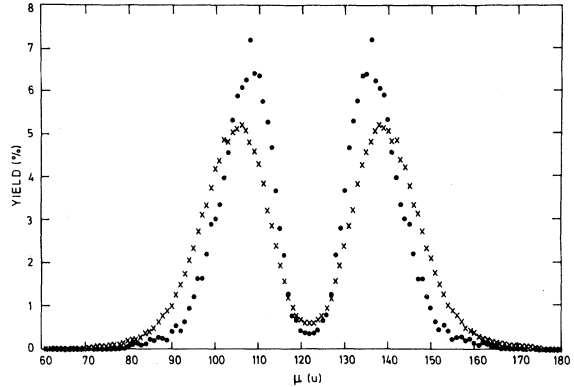


FIG. 7. Provisional mass distributions for the spontaneous (dots) and 20-MeV bremsstrahlung induced photofission (crosses) of ^{244}Pu .

masses of the light and heavy fragment peaks of the overall provisional and preneutron mass distributions are denoted by $\langle \mu_L \rangle$, $\langle \mu_H \rangle$ and $\langle m_L^* \rangle$, $\langle m_H^* \rangle$. The corresponding standard deviations are indicated by $\sigma(\mu_L)$ and $\sigma(\mu_H)$. As for the parameters of the kinetic energy distributions, the uncertainties on the average masses and standard deviations are the root-mean-square deviations for at least five experimental runs. The values for the peak-to-valley ratios of the provisional mass distributions P/V together with their statistical uncertainties are also given in Table I, although the absolute values of the asymmetric-to-symmetric fission yield ratios are rather senseless, especially for spontaneous fission, owing to the use of an electro-sprayed target. Table I shows that the average light and heavy fragment masses are practically independent of the end-point energy of the bremsstrahlung. However, for spontaneous fission a striking shift of 3 mass units of the average light and heavy fragment masses towards symmetry, compared to the photon induced fission case, is present. As was also observed for the fissioning systems ^{240}Pu (Ref. 2) and ^{242}Pu (Ref. 3), the width of the mass distribution peaks is significantly lower in the case of spontaneous fission than in photon and neutron induced fission.

The provisional mass distributions for the spontaneous fission and 20-MeV bremsstrahlung induced photofission of ^{244}Pu are presented in Fig. 7. This comparison shows the broadening and shift towards asymmetry of the mass distribution peaks, an increased yield in the symmetric fission region, and a strong decrease of the yield in the region around mass 135 for photofission. In the framework of the static scission point model, the latter effect can be attributed to a diminution at higher intrinsic temperatures of the importance of the shell-stabilized configuration in the $N=82$ mass region. The de-

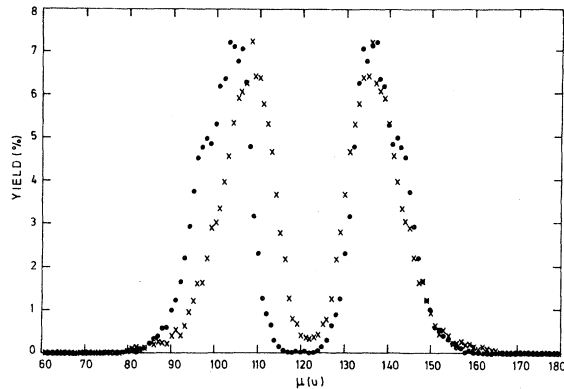


FIG. 8. Comparison of the provisional mass distributions for $^{240}\text{Pu}(\text{sf})$ and $^{244}\text{Pu}(\text{sf})$ represented by dots and crosses, respectively.

creased peak yield is only partially responsible for the increased width and general shift towards asymmetry of the mass distribution peaks at higher excitation energy. Calculations⁵ for different intrinsic temperatures of the fissioning system ^{244}Pu show that the broadening and shift towards asymmetry of the mass distribution peaks for increased excitation energy of the compound system cannot be understood in a simple static scission point model with a single choice for the parameters T_{coll} and d .

In Fig. 8 the provisional mass distributions for the spontaneous fission of ^{240}Pu and ^{244}Pu are compared. As generally observed, an increase of the compound nucleus neutron number results in a shift of the light fragment peak, while the heavy fragment peak remains essentially constant in position due to the strong influence of the spherical $N=82$ and deformed $N=88$ neutron shells. From Fig. 8 it is clear that the enhanced yield in the region around mass 142 observed in the spontaneous fission of ^{240}Pu is not present for the fissioning system ^{244}Pu .

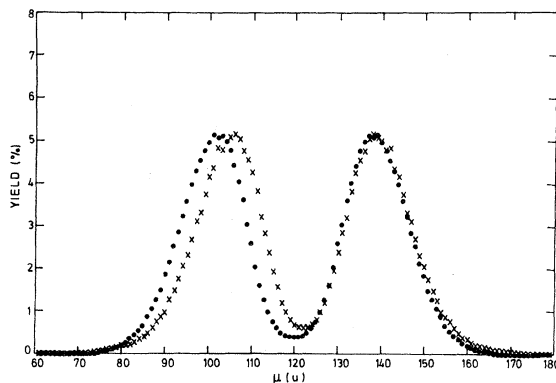


FIG. 9. Provisional mass distributions for 20-MeV bremsstrahlung induced photofission of ^{240}Pu (dots) and ^{244}Pu (crosses).

Scission point model calculations also reveal a shoulder in the mass distribution around mass 142 for the fissioning system ^{240}Pu which disappears for ^{244}Pu . This is owing to the relatively strong deformed neutron shell at $N=58$ (minimum B in the neutron shell correction-deformation surface, plotted in Fig. 1 of Ref. 1) in the light fragments, complementary in the case of the fissioning system ^{240}Pu to heavy fragments belonging to the strong deformed neutron shell at $N=88$.

The provisional mass distributions for the photofission of ^{240}Pu and ^{244}Pu with 20-MeV bremsstrahlung are compared in Fig. 9. This figure shows also that the increase of the neutron number of the fissioning nucleus results mainly in a shift of the light fragment peak. The difference between spontaneous fission and photon induced fission is only 1 mass unit for the fissioning system ^{240}Pu (see Ref. 2, Table I), while this difference is 3 mass units for the fissioning system ^{244}Pu . Scission point model calculations⁵ for different intrinsic temperatures do not reveal this difference between the fissioning systems ^{240}Pu and ^{244}Pu .

IV. CONCLUSIONS

The performed energy correlation measurements for the photon induced fission of ^{244}Pu at different bremsstrahlung end-point energies showed that changes in the kinetic energy release with the compound nucleus excitation energy are mainly due to a diminution of the shell corrections in the mass region of the spherical $N=82$ neutron shell, and that the fission degree of freedom is very weakly coupled to quasiparticle excitations. The comparison of the $\langle E_k^* \rangle(m^*)$ behavior for the spontaneous and 20-MeV bremsstrahlung induced fission also reveals changes in the deformation of the fragments in the $N=82$ mass region, but the observed increase of the kinetic energy in photofission for strongly asymmetric mass splits is difficult to attribute to changes in the shell corrections at higher intrinsic temperatures. The $\langle E_k^* \rangle(m_H^*)$ values for the spontaneous fission of ^{244}Pu lie about 3 MeV above the curve for the spontaneous fission of ^{240}Pu . This difference would suggest more compact scission shapes or/and a higher precession kinetic energy in the case of ^{244}Pu . It cannot be explained in a scission point model based on deformed-shell effects. Comparing the photofission results for the two fissioning systems ^{240}Pu and ^{244}Pu , the systematic difference in the $\langle E_k^* \rangle(m_H^*)$ values is reduced to 1 MeV.

Concerning the mass distribution in photofission compared to spontaneous fission, a decreased peak yield, a broadening of the mass distribution peaks, and a shift over 3 mass units towards asymmetry are

observed. This behavior can partially be explained by a diminution of shell corrections in the $N=82$ mass region. For both the spontaneous and photon induced fission of ^{240}Pu and ^{244}Pu , the heavy fragment peak remains practically constant in position.

ACKNOWLEDGMENTS

This research was supported by the Interuniversity Institute for Nuclear Science—National Fund for

Scientific Research. Professor Dr. A. J. Deruytter is acknowledged for his continuous interest. Thanks are expressed to the linac team of our laboratory for the operation of the accelerator and to Dr. R. Van de Vyver and Dr. E. Kerckhove for their aid during the cross section measurements. The authors are also indebted to Dr. M. Nève de Mévergnies, Dr. C. Wagemans, and Dr. E. Allaert for their help during the measurements at the SCK-CEN, Mol, Belgium.

-
- ¹B. D. Wilkins, E. P. Steinberg, and R. R. Chasman, *Phys. Rev. C* **14**, 1832 (1976).
- ²H. Thierens, A. De Clercq, E. Jacobs, D. De Frenne, P. D'hondt, P. De Gelder, and A. J. Deruytter, *Phys. Rev. C* **23**, 2104 (1981).
- ³E. Allaert, C. Wagemans, G. Wegener-Penning, A. J. Deruytter, and R. Barthélémy, *Nucl. Phys.* **A380**, 61 (1982).
- ⁴D. M. Crawford, R. Koch, and H. H. Thies, *Nucl. Instrum. Methods* **109**, 573 (1973).
- ⁵J. Moreau and K. Heyde, private communication.
- ⁶A. De Clercq, E. Jacobs, D. De Frenne, H. Thierens, P. D'hondt, and A. J. Deruytter, *Phys. Rev. C* **13**, 1536 (1976).
- ⁷H. W. Schmitt, W. E. Kiker, and C. E. Williams, *Phys. Rev.* **137**, B837 (1965).
- ⁸J. Neiler, F. Walter, and H. Schmitt, *Phys. Rev.* **149**, 894 (1966).
- ⁹N. S. Rabotnov, G. N. Smirenkin, A. S. Soldatov, L. N. Usachev, S. P. Kapitza, and Yu. M. Tsipenyuk, *Yad. Fiz.* **11**, 508 (1970) [*Sov. J. Nucl. Phys.* **11**, 285 (1970)].
- ¹⁰J. T. Caldwell, E. J. Dowdy, B. L. Berman, R. A. Alvarez, and P. Meyer, *Phys. Rev. C* **21**, 1215 (1980).
- ¹¹L. J. Schiff, *Phys. Rev.* **83**, 252 (1951).
- ¹²C. J. Orth, *Nucl. Sci. Eng.* **43**, 54 (1971).
- ¹³H. Nifenecker, C. Signarbieux, R. Babinet, and J. Poutou, in *Proceedings of the Third International Symposium on the Physics and Chemistry of Fission, Rochester, 1973* (IAEA, Vienna, 1974), Vol. II, p. 117.
- ¹⁴H. G. Clerc, W. Lang, H. Wohlfarth, H. Schrader, and K. H. Schmidt, in *Proceedings of the Fourth International Symposium on the Physics and Chemistry of Fission, Jülich, 1979* (IAEA, Vienna, 1980), Vol. II, p. 65.
- ¹⁵H. G. Clerc, W. Lang, H. Wohlfarth, K. H. Schmidt, H. Schrader, K. E. Pferdekämper, and R. Jungmann, *Z. Phys. A* **274**, 203 (1975).
- ¹⁶P. Möller and J. Nix, Los Alamos National Laboratory Report LA-UR-80-1996, 1980.
- ¹⁷F. Caitucoli, C. Wagemans, P. Perrin, E. Allaert, P. D'hondt, and M. Asghar, *Nucl. Phys.* **A369**, 15 (1981).
- ¹⁸J. P. Unik, J. E. Gindler, L. E. Glendenin, K. J. Flynn, A. Gorski, and R. K. Sjoblom, in *Proceedings of the Third International Symposium on the Physics and Chemistry of Fission, Rochester, 1973* (IAEA, Vienna, 1974), Vol. II, p. 19.
- ¹⁹H. A. Nifenecker, J. Blachot, J. P. Bocquet, R. Brissot, J. Crançon, C. Hamelin, G. Mariolopoulos, and C. Ristori, in *Proceedings of the Fourth International Symposium on the Physics and Chemistry of Fission, Jülich, 1979* (IAEA, Vienna, 1980), Vol. II, p. 35.